

# PSK Communication with Passband Additive Symmetric $\alpha$ -Stable Noise

Ahmed Mahmood, *Student Member, IEEE*, Mandar Chitre, *Senior Member, IEEE*,  
and Marc Andre Armand, *Senior Member, IEEE*

**Abstract**—The conventional additive white Gaussian noise (AWGN) model adequately simulates many noisy environments that hamper the performance of practical digital communication systems. However if the channel noise is impulsive, the approximation this model provides reduces significantly. The AWGN channel may then be replaced by the more general additive white symmetric  $\alpha$ -stable noise (AWS $\alpha$ SN) model. When converted to its complex baseband form, the resulting noise for the non-Gaussian AWS $\alpha$ SN case is radically different from its Gaussian counterpart. In this paper we investigate the properties of baseband noise for the general AWS $\alpha$ SN case using conventional passband-to-baseband conversion schemes. The converted noise is generally not isotropic and furthermore the real and imaginary components may be dependent. By varying certain physical parameters we may attain different non-isotropic distributions. Using the variable geometry offered by these distributions, efficient placement of signal points on the constellation map for the quadrature phase-shift keying (QPSK) scheme is proposed. It is shown that efficient placement of signal points significantly improve the uncoded error performance of the system. We plot the bit error rate (BER) and symbol error rate (SER) curves against a signal-to-noise ratio (SNR) measure for a few selected rotated versions of the QPSK scheme.

**Index Terms**—Impulsive noise, AWGN, AWS $\alpha$ SN, isotropic, QPSK.

## I. INTRODUCTION

THE justification of using the common *additive white Gaussian noise* (AWGN) channel stems from the *central limit theorem* (CLT) [1] which states that for a fixed power constraint, the sum of  $N$  independent and identically distributed (IID) random variables tends to a Gaussian distribution as  $N \rightarrow \infty$ . The AWGN model is a great approximation of the cumulative effect of random noise producing phenomenon encountered in practical communication scenarios. If however the noise is impulsive in nature, i.e., there are sudden high deviations (spikes) in the amplitude of subsequent noise samples, then the AWGN model does not work as well.

Gaussian random variables are part of a larger family called *stable* random variables. If the power constraint is removed from the CLT, the sum of  $N$  IID random variables then

tends to a stable distribution as  $N \rightarrow \infty$ . This is called the *generalized central limit theorem* (GCLT) [2]–[4]. The Cauchy random variable is another example that falls in this class of distributions. Due to the removal of the finite power constraint, stable non-Gaussian random variables simulate impulses much more effectively [3], [4]. It has already been shown in [4] that models based on stable distributions are effective in simulating impulsive noise scenarios. Stable distributions that are symmetric about zero are further termed as symmetric  $\alpha$ -stable (S $\alpha$ S), where  $\alpha$  is a parameter that determines the heaviness of their tails and hence the frequency of impulses. A zero-mean Gaussian distribution is a member of the S $\alpha$ S family. Impulsive noise environments have been approximated well by replacing the AWGN model by the more general additive white symmetric  $\alpha$ -stable noise (AWS $\alpha$ SN) channel [4]. AWS $\alpha$ SN has been used to model snapping shrimp noise encountered in shallow underwater scenarios [5]–[7]. Stable distributions have one significant drawback; with the exception of the Gaussian and Cauchy cases, a closed form probability density function (pdf) does not exist [2]–[4]. One has to adopt an alternate strategy when dealing with such variables. Efficient numerical techniques used to approximate these pdfs have been presented in [8], [9]. Gaussian mixture models in [10], [11] have been used to overcome this problem. In [12], Cauchy-Gaussian mixture models are presented to approximate the high tail probability in a more computationally intensive but relatively effective way.

Any random variable may be completely represented by its characteristic function (cf) instead of its distribution [13]. The cf of a random variable is the Fourier transform of its pdf. For the stable family of random variables, the cf exists in a nice closed form [2]–[4]. Like the univariate case, the multivariate stable case also does not have a closed form pdf. Further still, only a few certain sub-classes have a closed form joint-cf [3], [4]. In this paper we derive a general bivariate-cf for complex baseband stable noise in conventional passband-to-baseband conversion systems with the assumption that the passband noise is additive, white and S $\alpha$ S. We later see that the baseband noise is S $\alpha$ S. Using the derived expressions, we extract useful insight into the characteristics of the resultant noise. It is well known that the baseband noise derived from AWGN is isotropic and its components are IID Gaussian [13]. For the non-Gaussian AWS $\alpha$ SN case, the components may or may not be independent. Further still, the noise might not even be isotropic. In fact, by varying system parameters one may achieve a variety of baseband noise distributions. Due to these

Paper approved by E. Perrins, the Editor for Modulation Theory of the IEEE Communications Society. Manuscript received August 12, 2011; revised February 19, 2012.

A. Mahmood and M. A. Armand are with the Department of Electrical and Computer Engineering, National University of Singapore, Singapore 117576, Singapore (e-mail: {ahmed.mahmood, eleama}@nus.edu.sg).

M. Chitre is with the Department of Electrical and Computer Engineering and the ARL, Tropical Marine Science Institute, National University of Singapore, Singapore 119227, Singapore (e-mail: mandar@nus.edu.sg).

Digital Object Identifier 10.1109/TCOMM.2012.072412.110518

differences, techniques that are optimized for Gaussian noise scenarios might not be effective in the presence of impulsive noise.

This paper is organized as follows. In Section II we define notations and explain concepts that are relevant to the work we present in this paper. Our derivation and subsequent explanation of the bivariate characteristic function of complex baseband S $\alpha$ S noise is presented in Section III. We show simulation results in Section V. Finally, a summary of this paper is presented in Section VI.

## II. NOTATION AND CONCEPTS

This section is divided into three parts. Section II-A presents selected concepts about stable random variables and vectors. In Section II-B we explain the characteristics of the general AWS $\alpha$ SN channel. Finally, Section II-C briefly explains passband-to-baseband conversion in digital communication systems. We assume all vectors to be column vectors unless explicitly stated otherwise.

### A. S $\alpha$ S Variables and Vectors

A random variable  $X$  is classified as stable if and only if

$$aX_1 + bX_2 \stackrel{d}{=} cX + d \quad (1)$$

where  $X_1$  and  $X_2$  are IID copies of  $X$  and  $a$ ,  $b$ ,  $c$  and  $d$  are real numbers [2]. The symbol  $\stackrel{d}{=}$  implies equality in distribution. If  $d = 0$ , then  $X$  is termed as *strictly stable*. With the exception of the Gaussian and Cauchy cases, a closed form expression for the pdf of a stable random variable does not exist. On the other hand the cf of such a variable has a closed form [2], [3]. The cf  $\Phi_X(\theta)$  of a random variable  $X$  is the Fourier transform of its pdf and is calculated as  $E[\exp(i\theta X)]$  where  $E[\cdot]$  is the expectation operator and  $\theta$  is the frequency domain variable [13]. Because of their relationship, the cf is a suitable replacement for the pdf to statistically characterize any random variable. For stable random variables, there are different parameterizations of  $\Phi_X(\theta)$  which are summed up in [2], each of which have their own desirable properties. We stick to a commonly used convention [2], [3].

$$\Phi_X(\theta) = \begin{cases} \exp(-\delta^\alpha |\theta|^\alpha (1 - i\beta(\text{sign } \theta) \tan \frac{\pi\alpha}{2}) + i\mu\theta) & \text{for } \alpha \neq 1 \\ \exp(-\delta |\theta| (1 + i\beta \frac{2}{\pi} (\text{sign } \theta) \ln |\theta|) + i\mu\theta) & \text{for } \alpha = 1 \end{cases} \quad (2)$$

The parameters  $\alpha$ ,  $\beta$ ,  $\delta$  and  $\mu$  are real and completely define the distribution of  $X$  which in turn is denoted by  $\mathcal{S}(\alpha, \beta, \delta, \mu)$ .  $\alpha$  is the *characteristic exponent* and determines the heaviness of the tails for the distribution.  $\beta$ , the *skew parameter*, alters the symmetry.  $\delta$  controls the spread and is consequently termed the *scale parameter*. Finally, the value of  $\mu$  determines the position and is the *location parameter* of the distribution. The range of these parameters are listed below [3]:

- $\alpha \in (0, 2]$
- $\beta \in [-1, +1]$
- $\delta \in (0, +\infty)$
- $\mu \in (-\infty, +\infty)$

When  $\alpha = 2$ , (2) is the characteristic function of a Gaussian random variable with distribution  $\mathcal{N}(\mu, 2\delta^2)$ , where  $\mu$  and  $2\delta^2$  are the mean and variance of the distribution respectively [2]–[4]. Notice that when  $\alpha = 2$ , the skew parameter  $\beta$  is nullified and has no effect on the distribution. For  $\alpha = 1$  the cf in (2) is that of a Cauchy random variable.

A random variable is symmetric  $\alpha$ -stable (S $\alpha$ S) if  $\beta$  and  $\mu$  are equal to zero [3], [4]. The distribution of such a variable reduces to  $\mathcal{S}(\alpha, 0, \delta, 0)$ . The term ‘symmetric’ stems from the fact that  $f_X = f_{-X}$  where  $f_X$  is the distribution function of  $X$ . From the properties of the Fourier transform, this implies that  $\Phi_X(\theta)$  is real and symmetric about  $\theta$ , i.e.,  $\Phi_X(\theta) = \Phi_X(-\theta) = \Phi_X^*(\theta)$ . We can see this by plugging  $\beta = 0$  and  $\mu = 0$  in (2) to get the cf of  $X$  [3].

$$\Phi_X(\theta) = \exp(-\delta^\alpha |\theta|^\alpha) \quad (3)$$

Any S $\alpha$ S random variable is also strictly stable, the converse does not hold when  $\alpha = 1$ . Further still, any S $\alpha$ S variable is also classified as  $\alpha$ -sub-Gaussian [3], the converse is true too. An  $\alpha$ -sub-Gaussian and hence S $\alpha$ S variable can be represented as

$$X = A^{1/2}G \quad (4)$$

where  $G \sim \mathcal{N}(0, 2\delta^2)$  and  $A \sim \mathcal{S}(\alpha/2, 1, (\cos \frac{\pi\alpha}{4})^{2/\alpha}, 0)$  and are mutually independent. We notice that  $G$  is zero-mean Gaussian and  $A$  is a totally right-skewed random variable. We will now extend our discussion to the multivariate stable distribution case with emphasis on  $\alpha$ -sub-Gaussian random vectors.

The expression in (2) can be extended to define an  $N$ -dimensional stable random *vector*  $\vec{X}$  such that

$$a\vec{X}_1 + b\vec{X}_2 \stackrel{d}{=} c\vec{X} + d \quad (5)$$

where  $\vec{X}_1$  and  $\vec{X}_2$  are IID copies of  $\vec{X}$ . If  $d = 0$ , then  $\vec{X}$  is strictly stable. The joint-cf of a multi-variate stable random vector, unlike the univariate case, generally does not have a closed form. However, there are certain subclasses that are exceptions to this rule, with one of them being the  $\alpha$ -sub-Gaussian vector family [3]. The joint-cf of an  $N$ -dimensional random vector  $\vec{X}$  is given as

$$\Phi_{\vec{X}}(\vec{\theta}) = E \left[ \exp \left( i\vec{\theta}^T \vec{X} \right) \right] \quad (6)$$

where the elements of  $\vec{\theta}$  are  $\theta_i \forall i \in \{1, 2, \dots, N\}$  and  $\theta_i$  is the frequency domain variable corresponding to the distribution of the  $i^{\text{th}}$  element in  $\vec{X}$ . If  $\vec{X}$  is S $\alpha$ S, i.e.,  $f_{\vec{X}} = f_{-\vec{X}}$  where  $f_{\vec{X}}$  is the joint-distribution of  $\vec{X}$ , it is also strictly stable. The converse is not true. Further still, the cf of  $\vec{X}$  will then be real and symmetric about  $\vec{\theta}$ , i.e.,  $\Phi_{\vec{X}}(\vec{\theta}) = \Phi_{\vec{X}}(-\vec{\theta}) = \Phi_{\vec{X}}^*(\vec{\theta})$ . Like the univariate case,  $\alpha$ -sub-Gaussian implies that  $\vec{X}$  is symmetric. The converse however is not true. We may decompose an  $\alpha$ -sub-Gaussian vector  $\vec{X}$  as

$$\vec{X} = A^{1/2}\vec{G} \quad (7)$$

where  $A$  is a random variable with distribution  $\mathcal{S}(\alpha/2, 1, (\cos \frac{\pi\alpha}{4})^{2/\alpha}, 0)$  and  $\vec{G}$  is a zero-mean Gaussian random vector of dimension equal to that of  $\vec{X}$ .

The density of  $\vec{X}$  in (7) shares structural similarities with that of the underlying Gaussian vector. For e.g., an  $N$ -dimensional non-degenerate  $\alpha$ -sub-Gaussian vector implies an underlying non-degenerate  $N$ -dimensional Gaussian vector and will have its equiprobable density surfaces shaped as  $N$ -dimensional ellipsoids. These surfaces become spherical if the elements of the underlying Gaussian vector are IID. This concept may be extended to the degenerate case. Also note that due to  $A$  in (7), the elements of  $\vec{X}$  will always be dependent, irrespective of the elements of  $\vec{G}$  being independent or dependent [3]. The cf of  $\vec{X}$  is further given as

$$\Phi_{\vec{X}}(\vec{\theta}) = \exp\left(-\left|\frac{1}{2}\vec{\theta}^t \mathbf{R} \vec{\theta}\right|^{\alpha/2}\right) \quad (8)$$

where  $\mathbf{R}$  is the covariance matrix of  $\vec{G}$  and  $\alpha$  is the characteristic exponent of  $\vec{X}$ . For  $\alpha = 1$  and  $\alpha = 2$  the joint cf in (8) reduces to that of an  $\alpha$ -sub-Gaussian Cauchy and a zero-mean Gaussian vector, respectively.

The concepts presented till now provide a sufficient platform to understand the rest of this paper. For further details on stable random variables and vectors, we refer the reader to Samorodnitsky and Taqqu [3].

### B. The AWS $\alpha$ SN Channel

The AWS $\alpha$ SN channel has been used in the literature to model impulsive noise [5]–[7]. The noise samples of an AWS $\alpha$ SN channel are real and IID. We denote these samples by  $N(n)$  where  $n$  is the discrete-time index. When  $\alpha = 2$ , the more general AWS $\alpha$ SN channel reduces to the AWGN model. The term ‘white’ implies a flat power spectral density (PSD) spanning over all frequencies for the Gaussian case. It should be noted that this definition does not hold when associated with non-Gaussian AWS $\alpha$ SN. This is due to the fact that second-order moments of stable non-Gaussian distributions are infinite [3], [4]. The term is maintained because it asserts independence of noise samples in AWGN which is what is implied in the case of non-Gaussian AWS $\alpha$ SN. We further note that the distribution of any individual sample at any time for the AWS $\alpha$ SN channel is  $\mathcal{S}(\alpha, 0, \delta_p, 0)$ . For the Gaussian case this is equivalent to  $\mathcal{N}(0, 2\delta_p^2)$ . As we will later see, the notation  $\delta_p$  is used so that we do not confuse the passband distribution parameters with those of the baseband. If we let  $\vec{N}$  be an  $L$ -dimensional vector whose elements  $N(n) \forall n \in \{1, 2, \dots, L\}$  are time-samples of an AWS $\alpha$ SN channel, then the joint-cf of  $\vec{N}$  for any  $\alpha$  is given as:

$$\begin{aligned} \Phi_{\vec{N}}(\vec{\theta}) &= \prod_{i=1}^L \Phi_{N(n)}(\theta_i) \\ &= \prod_{i=1}^L \exp(\delta_p^\alpha |\theta_i|^\alpha) \\ &= \exp\left(\delta_p^\alpha \sum_{i=1}^L |\theta_i|^\alpha\right) \end{aligned} \quad (9)$$

We get (9) by utilizing the expression in (3). On comparison with (8) we see the joint-cf in (9) is not sub-Gaussian. However as the joint-cf is real and symmetric about  $\vec{\theta}$ , we state that  $\vec{N}$  is S $\alpha$ S.

### C. Passband to Baseband

The relationship of a discrete-time passband signal  $s(n)$ , indexed by  $n$ , to its upsampled baseband form  $z(n)$  is represented by the well known expression [1]

$$s(n) = \Re\left\{z(n) \exp\left(i2\pi \frac{f_c}{f_s} n\right)\right\} \quad (10)$$

where  $f_c$  and  $f_s$  are the carrier and passband sampling frequencies, respectively. The same relationship also holds if  $s(n)$  and hence  $z(n)$  are random processes. In addition however, we need to associate a joint-pdf with either of these signals. Adhering to convention in standard texts [1], [13], we use capitalized letters to represent random processes. We have already defined  $N(n)$  to be samples of a real passband AWS $\alpha$ SN process, we further state  $Z(n)$  to be its upsampled baseband counterpart.

$$N(n) = \Re\left\{Z(n) \exp\left(i2\pi \frac{f_c}{f_s} n\right)\right\} \quad (11)$$

To convert a passband signal to its baseband form, one essentially has to shift the signal by  $f_c$  in the spectral domain and pass the result through a low pass filter, the impulse response of which we denote by  $h(n)$ . We assume the filter to be an  $M$ -tap finite impulse response (FIR) filter with bandwidth equal to the normalized message signal bandwidth  $B/f_s$  where  $B$  is the baseband sampling frequency. We further assume the order of the filter, and hence  $M$ , to be high. Also,  $f_s > 2f_c + B$ . The shifting operation can be represented mathematically as

$$\begin{aligned} Z^+(n) &= N(n) e^{-i2\pi \frac{f_c}{f_s} n} \\ &= [\cos(2\pi \frac{f_c}{f_s} n) - i \sin(2\pi \frac{f_c}{f_s} n)] N(n) \end{aligned} \quad (12)$$

We write (12) in vector form as

$$\vec{Z}^+(n) = \begin{bmatrix} \vec{Z}_R^+(n) \\ \vec{Z}_I^+(n) \end{bmatrix} = \begin{bmatrix} \cos(2\pi \frac{f_c}{f_s} n) \\ -\sin(2\pi \frac{f_c}{f_s} n) \end{bmatrix} N(n) \quad (13)$$

where  $Z_R^+(n)$  and  $Z_I^+(n)$  are the real and imaginary components of  $\vec{Z}^+(n)$ , respectively. We use the  $+$  symbol in our notation to highlight that the positive band of the passband signal is shifted to zero. The subsequent filtering operation is expressed as

$$Z(n) = 2 \sum_{k=0}^{M-1} h(k) Z^+(n-k)$$

The scale factor of 2 is appended so that the relationship in (11) is maintained [1].  $Z(n)$  is complex and can be written in vector form as well:

$$\begin{aligned} \vec{Z}(n) &= \begin{bmatrix} Z_R(n) \\ Z_I(n) \end{bmatrix} \\ &= 2 \sum_{k=0}^{M-1} h(k) \begin{bmatrix} Z_R^+(n-k) \\ Z_I^+(n-k) \end{bmatrix} \\ &= 2 \sum_{k=0}^{M-1} h(k) \vec{Z}^+(n-k) \end{aligned} \quad (14)$$

It is further assumed that  $Z(n)$  is downsampled by a factor of  $f_s/B$  to get the actual baseband signal  $Z_b(n)$ , i.e.,  $Z_b(n) =$

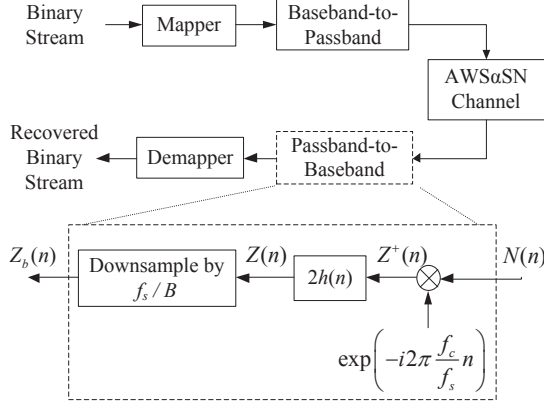


Fig. 1. A schematic of an uncoded digital communication system with AWS $\alpha$ SN along with a descriptive block diagram of the passband-to-baseband conversion block.

$Z(f_s n/B)$ . Similarly, in vector form  $\vec{Z}_b(n) = \vec{Z}(f_s n/B)$ . The real and imaginary components of  $Z_b(n)$  are  $Z_{R_b}(n)$  and  $Z_{I_b}(n)$ , respectively.

A schematic for an uncoded digital communication system is shown in Fig. 1 along with an elaborate diagram of the passband-to-baseband conversion block. The mapper converts a sequence of  $m$  information bits to a symbol that is represented as a signal point on a constellation diagram. The total number of symbols is consequently assumed to be  $2^m$ . The operation of the demapper is the inverse of the mapper.

### III. COMPLEX BASEBAND S $\alpha$ S NOISE

In this section we derive the bivariate characteristic function of complex baseband S $\alpha$ S noise with the assumption that the passband noise is AWS $\alpha$ SN. We will first characterize  $\vec{Z}^+(n)$ . On the basis of that we will derive the cf of  $\vec{Z}(n)$  and  $\vec{Z}_b(n)$ . As all passband samples  $N(n)$  are individually sub-Gaussian, using (4) we can decompose each sample into

$$N(n) = A^{\frac{1}{2}}(n)G(n) \quad (15)$$

where  $A(n) \sim \mathcal{S}(\frac{\alpha}{2}, 1, (\cos \frac{\pi\alpha}{4})^{2/\alpha}, 0)$  and  $G(n) \sim \mathcal{N}(0, 2\delta_p^2)$  are independent of each other. As the samples  $N(n)$  are IID, so will be the samples  $A(n)$  and  $G(n)$  for all  $n$ .

*Proposition 1:* For any  $n$  and  $\alpha \in (0, 2]$ ,  $\vec{Z}^+(n)$  is  $\alpha$ -sub-Gaussian with the covariance matrix of the underlying Gaussian vector  $\hat{G}(n)$  being:

$$\mathbf{R}(n) = 2\delta_p^2 \begin{bmatrix} \cos^2(2\pi \frac{f_c}{f_s} n) & -\frac{1}{2} \sin(4\pi \frac{f_c}{f_s} n) \\ -\frac{1}{2} \sin(4\pi \frac{f_c}{f_s} n) & \sin^2(2\pi \frac{f_c}{f_s} n) \end{bmatrix} \quad (16)$$

*Proof:* By substituting (15) in (13) we get

$$\begin{aligned} \vec{Z}^+(n) &= \begin{bmatrix} \cos\left(2\pi \frac{f_c}{f_s} n\right) \\ -\sin\left(2\pi \frac{f_c}{f_s} n\right) \end{bmatrix} N(n) \\ &= A^{\frac{1}{2}}[n] \begin{bmatrix} \cos\left(2\pi \frac{f_c}{f_s} n\right) \\ -\sin\left(2\pi \frac{f_c}{f_s} n\right) \end{bmatrix} G(n) \\ &= A^{\frac{1}{2}}[n] \hat{G}(n) \end{aligned} \quad (17)$$

where

$$\hat{G}(n) = \begin{bmatrix} \cos\left(2\pi \frac{f_c}{f_s} n\right) \\ -\sin\left(2\pi \frac{f_c}{f_s} n\right) \end{bmatrix} G(n)$$

We see that  $\hat{G}(n)$  is zero-mean bivariate Gaussian which makes  $\vec{Z}^+(n)$  sub-Gaussian. The covariance matrix of  $\hat{G}(n)$  is calculated by evaluating  $\mathbf{R}(n) = E[\hat{G}(n)\hat{G}(n)^T]$ , which results in (16).  $\square$

We observe from the covariance matrix in (16) that  $\hat{G}(n)$  and hence  $\vec{Z}^+(n)$  are degenerate.

*Corollary 1:* The characteristic function of  $\vec{Z}^+(n)$  is

$$\Phi_{\vec{Z}^+(n)}(\vec{\theta}) = \exp\left(-\left|\frac{1}{2}\vec{\theta}^t \mathbf{R}(n) \vec{\theta}\right|^{\alpha/2}\right) \quad (18)$$

*Proposition 2:* For any  $n$  and  $\alpha \in (0, 2]$ , the random vector  $\vec{Z}(n)$  is S $\alpha$ S and has the following joint-cf:

$$\Phi_{\vec{Z}(n)}(\vec{\theta}) = \exp\left(-\sum_{k=0}^{M-1} \left|2h^2(k)\vec{\theta}^t \mathbf{R}(n-k)\vec{\theta}\right|^{\alpha/2}\right) \quad (19)$$

*Proof:* We use (14) and the whiteness of passband noise samples to get:

$$\begin{aligned} \Phi_{\vec{Z}(n)}(\vec{\theta}) &= E\left[\exp\left(i\vec{\theta}^t \vec{Z}(n)\right)\right] \\ &= E\left[\exp\left(i2 \sum_{k=0}^{M-1} h(k)\vec{\theta}^t \vec{Z}^+(n-k)\right)\right] \\ &= \prod_{k=0}^{M-1} E\left[\exp\left(i2h(k)\vec{\theta}^t \vec{Z}^+(n-k)\right)\right] \\ &= \prod_{k=0}^{M-1} E\left[\exp\left(i\left(2h(k)\vec{\theta}\right)^t \vec{Z}^+(n-k)\right)\right] \end{aligned} \quad (20)$$

Using (18), (20) becomes

$$\begin{aligned} \Phi_{\vec{Z}(n)}(\vec{\theta}) &= \prod_{k=0}^{M-1} \exp\left(-\left|2h^2(k)\vec{\theta}^t \mathbf{R}(n-k)\vec{\theta}\right|^{\alpha/2}\right) \\ &= \exp\left(-\sum_{k=0}^{M-1} \left|2h^2(k)\vec{\theta}^t \mathbf{R}(n-k)\vec{\theta}\right|^{\alpha/2}\right) \end{aligned} \quad (21)$$

To see if the distribution of  $\vec{Z}(n)$  is bivariate S $\alpha$ S, we merely note that (21) is real and symmetric about  $\vec{\theta}$ .  $\square$

*Corollary 2:* The cfs of the marginal distributions of  $\vec{Z}[n]$  are

$$\begin{aligned} \Phi_{Z_R(n)}(\theta) &= \\ \exp\left(-\sum_{k=0}^{M-1} \left|4h^2(k)\theta^2 \cos^2\left(2\pi \frac{f_c}{f_s}(n-k)\right) \delta_p^2\right|^{\alpha/2}\right) \end{aligned} \quad (22)$$

$$\begin{aligned} \Phi_{Z_I(n)}(\theta) &= \\ \exp\left(-\sum_{k=0}^{M-1} \left|4h^2(k)\theta^2 \sin^2\left(2\pi \frac{f_c}{f_s}(n-k)\right) \delta_p^2\right|^{\alpha/2}\right) \end{aligned} \quad (23)$$

From (3), (22) and (23), we note that both  $Z_R(n)$  and  $Z_I(n)$  are SaS random variables. Their scale parameters are

$$\delta_{Z_R(n)} = \left( \sum_{k=0}^{M-1} \left| 2h(k) \cos \left( 2\pi \frac{f_c}{f_s} (n-k) \right) \delta_p \right|^\alpha \right)^{1/\alpha} \quad (24)$$

$$\delta_{Z_I(n)} = \left( \sum_{k=0}^{M-1} \left| 2h(k) \sin \left( 2\pi \frac{f_c}{f_s} (n-k) \right) \delta_p \right|^\alpha \right)^{1/\alpha} \quad (25)$$

respectively.

It is observed that the relationship between the cfs of  $Z_b(n)$  and  $Z(n)$ , i.e.,  $\Phi_{\bar{Z}_b(n)}(\vec{\theta}) = \Phi_{\bar{Z}(f_s n/B)}(\vec{\theta})$ , extends to the marginal distributions of  $Z_b(n)$  corresponding to (22) and (23).

*Example 1: (The AWGN Case)* The validity of the joint-cf in (19) and its marginals in (22) and (23) may be verified by applying the results to the Gaussian ( $\alpha=2$ ) case. The following facts of the resulting baseband noise are already known [1]:

- 1) For a given sample  $Z(n)$ , the real and imaginary components are IID. Hence, the bivariate distribution of any complex baseband sample is isotropic.
- 2) All complex baseband samples  $Z_b(n)$  are IID. Hence, the distribution does not vary with time.

We first calculate the cf of the marginal distribution of  $Z_R(n)$  for this case:

$$\begin{aligned} \Phi_{Z_R(n)}(\theta) &= \exp \left( - \sum_{k=0}^{M-1} \left| 4h^2(k)\theta^2 \cos^2 \left( 2\pi \frac{f_c}{f_s} (n-k) \right) \delta_p^2 \right| \right) \\ &= \exp \left( - \sum_{k=0}^{M-1} 4h^2(k)\theta^2 \cos^2 \left( 2\pi \frac{f_c}{f_s} (n-k) \right) \delta_p^2 \right) \\ &= \exp \left( - 4\theta^2 \delta_p^2 \underbrace{\sum_{k=0}^{M-1} h^2(k) \cos^2 \left( 2\pi \frac{f_c}{f_s} (n-k) \right)}_{\text{convolution}} \right) \end{aligned} \quad (26)$$

We know that  $h(n)$  is a fixed low-pass filter which allows frequencies within  $[-\frac{B}{2f_s}, \frac{B}{2f_s}]$  to pass through.  $h^2(n)$  is in essence also a low-pass filter. The magnitude of the frequency response of  $h^2(n)$  is a *triangular* function scaled by  $B/f_s$  and lies within  $[-B/f_s, B/f_s]$ . Looking at the convolution term in (26), we see that  $h^2(n)$  succeeds to terminate the high frequency component in  $\cos^2(2\pi \frac{f_c}{f_s} n) = \cos(4\pi \frac{f_c}{f_s} n)/2 + 1/2$  and retains the d.c term after scaling it by  $B/f_s$ . This reduces (26) to:

$$\Phi_{Z_R(n)}(\theta) = \Phi_{Z_R}(\theta) = \exp \left( - \frac{2B\delta_p^2\theta^2}{f_s} \right) \quad (27)$$

Using the same arguments we also evaluate

$$\Phi_{Z_I(n)}(\theta) = \Phi_{Z_I}(\theta) = \exp \left( - \frac{2B\delta_p^2\theta^2}{f_s} \right) \quad (28)$$

We see that the individual distributions of the real and imaginary components of  $Z(n)$  coincide with  $\mathcal{N}(0, 4B\delta_p^2/f_s)$ . Also, the marginal cfs are independent of the sample index  $n$ ,

highlighting the fact that the distributions of the components of  $\bar{Z}(n)$  do not vary with time. We can substitute  $\delta_p^2$  by  $N_0 f_s/4$  in (27) and (28) where  $N_0/2$  is the two-sided PSD of the passband AWGN process to get the baseband marginal cfs in terms of  $N_0$ .

$$\Phi_{Z_R}(\theta) = \Phi_{Z_I}(\theta) = \exp \left( - \frac{BN_0\theta^2}{2} \right) \quad (29)$$

Now to see if the real and imaginary parts of  $Z(n)$  are mutually independent at any  $n$ , we apply the same principle used in simplifying the convolution term in (26) to the joint-characteristic function in (19) and use the fact that  $\mathbf{R}(n)$  is positive semi-definite.

$$\begin{aligned} \Phi_{\bar{Z}(n)}(\vec{\theta}) &= \exp \left( - \sum_{k=0}^{M-1} \left| 2h^2(k)\vec{\theta}^T \mathbf{R}(n-k)\vec{\theta} \right| \right) \\ &= \exp \left( - 4\theta_1^2 \delta_p^2 \underbrace{\sum_{i=0}^{M-1} h^2(i) \cos^2 \left( 2\pi \frac{f_c}{f_s} (n-i) \right)}_{=B/2f_s} \right) \\ &\times \exp \left( - 4\theta_2^2 \delta_p^2 \underbrace{\sum_{i=0}^{M-1} h^2(i) \sin^2 \left( 2\pi \frac{f_c}{f_s} (n-i) \right)}_{=B/2f_s} \right) \\ &\times \exp \left( 4\theta_1\theta_2 \delta_p^2 \underbrace{\sum_{i=0}^{M-1} h^2(i) \sin \left( 4\pi \frac{f_c}{f_s} (n-i) \right)}_{=0} \right) \\ &= \exp \left( - \frac{2B\delta_p^2\theta_1^2}{f_s} - \frac{2B\delta_p^2\theta_2^2}{f_s} \right) \\ &= \Phi_{Z_R}(\theta_1)\Phi_{Z_I}(\theta_2) \end{aligned} \quad (30)$$

So the real and imaginary components of  $Z(n)$  for any  $n$  are also independent. We further see that  $\Phi_{\bar{Z}(n)}(\vec{\theta})$  is independent of  $n$ , thus showing that the bivariate distribution of all baseband samples are identical.

Finally, we note that the impulse response of the FIR filter is of the form

$$h(n) = \frac{B}{f_s} \text{sinc} \left( \frac{Bn}{f_s} \right) \quad (31)$$

where *sinc* is the *normalized sinc* function. Without loss of generality we assume the response to be noncausal and of infinite length. From (31), when  $n$  is a multiple of  $f_s/B$ , the impulse response  $h(n) = 0$  except at  $n = 0$ . The baseband samples are mutually independent because of the whiteness of passband samples, the placement of nulls in the impulse response  $h(n)$  and the fact that we downsample by  $f_s/B$  after filtering to generate the baseband signal. The passband samples  $N(n-k) \forall k \in \{0, 1, \dots, M-1\}$  that generate  $Z_b(n)$  via the filtering operation are nullified for any other baseband sample by  $h(n)$ , thus there is no same passband sample that generates any two or more baseband samples. We consequently state that all baseband samples are independent

of each other. The properties of complex baseband AWGN have been completely supported by our expressions.

We will now focus on the non-Gaussian scenario. The reasoning used to infer independence of all baseband samples  $Z_b(n)$  in the Gaussian example can be extended to other values of  $\alpha$  as well. We thus state that all samples  $Z_b(n)$  are independent of each other for any  $\alpha$ .

To see if the baseband samples are identical, the expression in (19) may be rewritten as

$$\begin{aligned} \ln(\Phi_{\vec{Z}(n)}(\vec{\theta})) &= - \sum_{k=0}^{M-1} \left| 2h^2(k)\vec{\theta}^t \mathbf{R}(n-k)\vec{\theta} \right|^{\alpha/2} \\ &= -p(n) * q(n) \end{aligned} \quad (32)$$

where

$$p(n) = |2h^2(n)|^{\alpha/2} \quad (33)$$

$$q(n) = \left| \vec{\theta}^t \mathbf{R}(n)\vec{\theta} \right|^{\alpha/2} \quad (34)$$

and  $*$  represents the convolution operator. Using (31),  $p(n)$  becomes

$$p(n) = \left| \frac{\sqrt{2}B}{f_s} \text{sinc} \left( \frac{Bn}{f_s} \right) \right|^{\alpha} \quad (35)$$

It is observed that  $p(n)$  is in essence a low-pass filter. To depict this, the magnitude response of  $p(n)$  for  $\alpha = 1$  and 2 are presented in Fig. 2(a) with  $f_s = 21$ ,  $f_c = 4$ ,  $B = 1$  and  $M = 800$ . The low-pass characteristics of  $p(n)$  may be extended to other values of  $\alpha$ . We also note that  $q(n)$  is a periodic signal as the term  $\vec{\theta}^t \mathbf{R}(n)\vec{\theta}$  in (34) may be expanded as

$$\begin{aligned} q(n) &= \left| 2\delta_p^2 \left( \theta_1^2 \cos^2 \left( 2\pi \frac{f_c}{f_s} n \right) + \theta_2^2 \sin^2 \left( 2\pi \frac{f_c}{f_s} n \right) \right. \right. \\ &\quad \left. \left. - \theta_1 \theta_2 \sin \left( 4\pi \frac{f_c}{f_s} n \right) \right) \right|^{\alpha/2} \end{aligned} \quad (36)$$

Any function of a periodic signal is periodic as well and in turn may be represented as a Fourier series. It should be noted that the number of harmonics of  $q(n)$  is equivalent to  $f_s/\text{gcd}(4f_c, f_s)$  (where  $\text{gcd}$  is the *greatest common divisor*) and does not depend on  $\alpha$ ,  $\vec{\theta}$  and/or  $\delta_b$ . For  $\theta_1 = \theta_2 = 1$  and  $\delta_b = 1$ , we have plotted the magnitude response of  $q(n)$  for the Cauchy case in Fig. 2(b). The result in (32) may be visualized as the multiplication of the respective frequency responses of  $p(n)$  and  $q(n)$ . For any combination of  $\vec{\theta}$ , it has been evaluated that the convolution in (32) (after subsequent downsampling) is independent of  $n$ , i.e., all harmonics of  $q(n)$  are effectively suppressed. This can be seen from the instances of the magnitude frequency response of  $p(n)$  and  $q(n)$  presented in Fig. 2. Thus the distribution of all samples  $Z_b(n)$  are identical.

In the Gaussian case, it was determined that the real and imaginary components of  $Z_b(n)$  are always independent. This is generally not true for non-Gaussian baseband  $S\alpha S$  noise. For the components of  $Z_b(n)$  to be independent, (19) has to break up into a product of its two marginal cfs in (22) and (23).

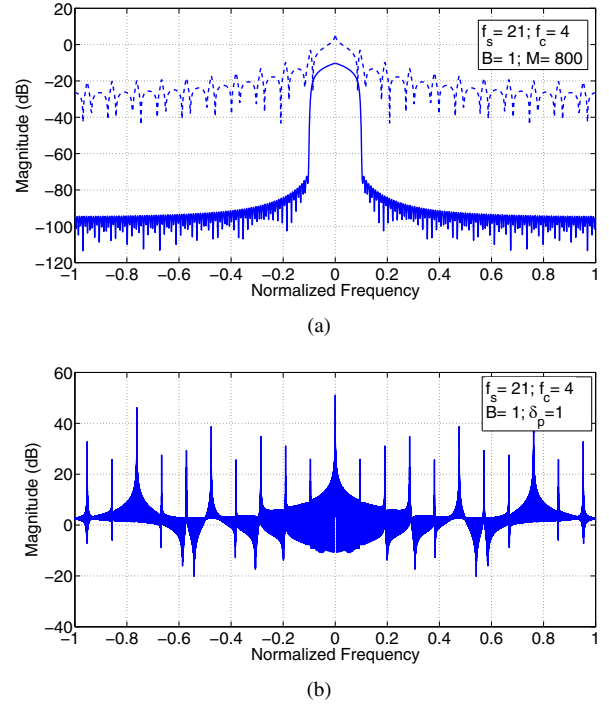


Fig. 2. In part (a), the magnitude frequency response of  $p(n)$  for the Gaussian case (solid line) and the Cauchy case (dashed line) are shown. Part (b) presents the magnitude response of  $q(n)$  for the Cauchy case with  $\theta_1 = \theta_2 = 1$ .

*Corollary 3:* For any given sample  $Z_b(n)$ , the real and imaginary components are independent if and only if  $f_s = 4f_c$ .

Corollary 3 follows from the fact that only for  $f_s = 4f_c$  does the matrix  $\mathbf{R}(n)$  in (19) become diagonal for any  $n$ . Further still, only one of the diagonal elements will be non-zero at any  $n$ . The joint-cf then reduces to the product of its marginal cfs which proves independence of components. It is necessary that we reiterate our assumption of  $M$  being large.

A question pertaining to the structure of the bivariate pdf of non-Gaussian  $\vec{Z}_b(n)$  arises, which unlike the Gaussian case (isotropic), varies for different ratios of  $f_c/f_s$ . An intuitive look into the expression in (13) reveals that the joint-pdf of  $\vec{Z}^+(n)$  is degenerate and lies along an angle of  $2\pi \frac{f_c}{f_s} n$  from the positive real axis. The filtering operation in (14) essentially scales and sums the independent complex samples  $\vec{Z}^+(n)$ , which results in a 2-dimensional convolution of these rotated degenerate pdfs. Due to the heavy tail phenomenon accompanying stable random variables, one would expect the resultant bivariate pdf of  $\vec{Z}(n)$  to have tails along angles that are multiples of  $2\pi f_c/f_s$  from the positive real axis. Assuming the ratio  $f_c/f_s$  to be a rational number (as in practical scenarios), the number of tails will be finite and will be uniformly distributed around the origin, hence resulting in non-isotropic distributions. The angle between the tails is given as

$$\psi_b = \begin{cases} \frac{2\pi \text{gcd}(f_c, f_s)}{f_s} & \text{if } f_s \text{ is an even multiple of } f_c \\ \frac{\pi \text{gcd}(f_c, f_s)}{f_s} & \text{otherwise} \end{cases} \quad (37)$$

Fig. 3 presents the bivariate density functions for the Cauchy case ( $\alpha = 1$ ). The different system parameters used

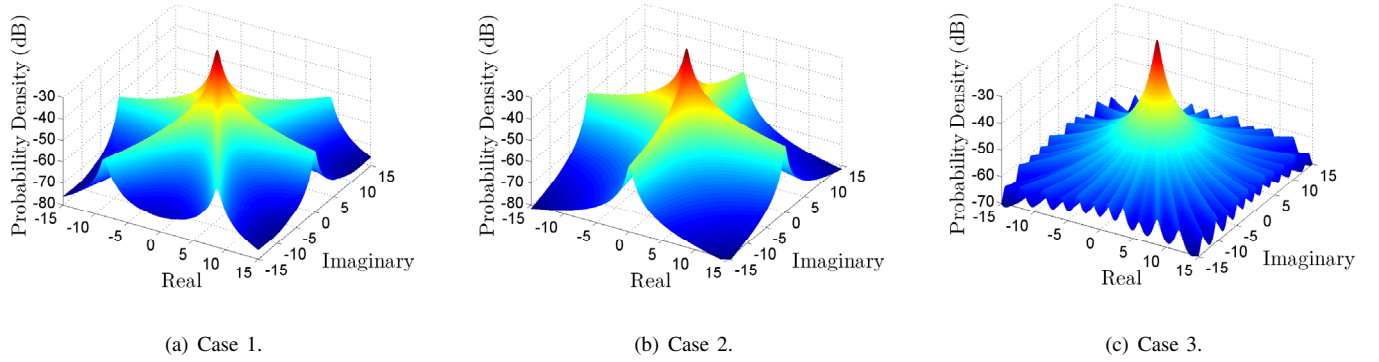


Fig. 3. Bivariate pdfs of complex baseband  $S\alpha S$  noise are presented for the Cauchy case ( $\alpha = 1$ ) under the assumption that the passband noise is AWS $\alpha$ SN. The parameters that generate each of these plots are summarized in Table I.

TABLE I  
PARAMETER SETTINGS FOR GENERATING THE DENSITY FUNCTIONS IN FIG. 3.

Case	$f_c$	$f_s$	$\text{gcd}(f_c, f_s)/f_s$	$B$
1.	4	12	1/3	1
2.	4	16	1/4	1
3.	4	21	1/21	1

to obtain these plots are summarized in Table I. For all cases, the order of the FIR filter was 800. The pdfs were evaluated by taking the inverse Fourier transform of (19). For Fig. 3(b) the real and imaginary components are independent following Corollary 3. For the other two cases, the real and imaginary parts are dependent. In Fig. 3(c), the baseband noise is near-isotropic.

On a final note, it has been observed that the marginal distributions of  $\vec{Z}_b(n)$ , although do not vary with time, are also *not* exactly identical. They are only identical if there exists a tail along the imaginary axis as in Case 2. or if the number of tails is large, i.e.,  $\psi_b$  is small. One way to get around this is by modifying the definition of a baseband signal in (10) to  $s(n) = \Re \left\{ z(n) \exp \left( i \left( 2\pi \frac{f_c}{f_s} n - \frac{\pi}{4} \right) \right) \right\}$ . This ensures that the tails of the bivariate distribution are uniformly distributed about both the real and imaginary axis.

Communication schemes optimized for the AWGN channel will not be optimum in the case of non-isotropic  $S\alpha S$  baseband noise. The next section illustrates the effect of such non-isotropic noise on communication system design.

#### IV. DECISION BOUNDARIES

In this section we depict the optimum decision regions on the constellation map for the quadrature phase-shift keying (QPSK) scheme for complex baseband  $S\alpha S$  noise. We focus on the case where the real and imaginary components of  $Z_b(n)$  are independent. This is mainly due to the lower error probabilities one would expect to achieve in comparison with other cases and also due to the availability of an easily evaluable joint-cf. We present a simple argument to support this statement. The joint entropy of a baseband noise sample

$Z_b(n)$  for any  $n$  is represented as

$$H(Z_{R_b}(n), Z_{I_b}(n)) = H(Z_{R_b}(n)) + H(Z_{I_b}(n)) - I(Z_{R_b}(n); Z_{I_b}(n)) \quad (38)$$

where  $H(X)$  is the entropy of  $X$  and  $I(X; Y)$  is the mutual information between  $X$  and  $Y$ . Assuming that no information is lost in passband-to-baseband conversion, the joint entropy should be the same regardless of any combination of system parameters. If the components of  $Z_b(n)$  are independent,  $I(Z_{R_b}(n); Z_{I_b}(n)) = 0$ . This implies that for a given joint entropy, the sum of individual entropies of the real and imaginary parts for the independent case will be lower than those of any dependent case. Further still,  $H(Z_{R_b}(n))$  and  $H(Z_{I_b}(n))$  are identical for the case of independent components. In conventional QPSK decoding, the I and Q channels are separately decoded. Assuming Gray coding, one would then expect lower error rates for the independent case due to lower noise entropies of its real and imaginary components.

It is known that the baseband noise derived from passband AWGN is isotropic [1]. The optimal decision boundaries for isotropic baseband noise are evaluated from the Euclidean distance between signal points. This implies that for a given constellation map and any one of its *rotated* version, there is no advantage in terms of error rate between them as the optimum decision boundaries rotate accordingly. By a ‘rotated version’ we imply that all signal points in the constellation have been rotated by a similar angle. The same deductions do not hold for the non-Gaussian case, as the bivariate distribution of  $\vec{Z}_b(n)$  will not be isotropic (assuming  $f_c/f_s$  is rational). Intuitively, one would want to position the signal points in such a way that the tails of the baseband distribution are not directed towards any signal point.

In Fig. 4 we show the optimal decision regions for QPSK and its rotated versions for the independent component case for  $\alpha = 1$ . We denote these schemes as QPSK- $\phi$  where  $\phi$  is the angle (in radians) of the signal point in the first quadrant from the positive real axis. The signal points are signified by the red dots on the constellation map. The regions are calculated via the maximum likelihood (ML) detection rule. It is assumed that the scale parameters in (24) and (25) are equal to one and the transmitted signals lie on the unit circle. We note that the decision regions in Fig. 4(b) are the same as the isotropic

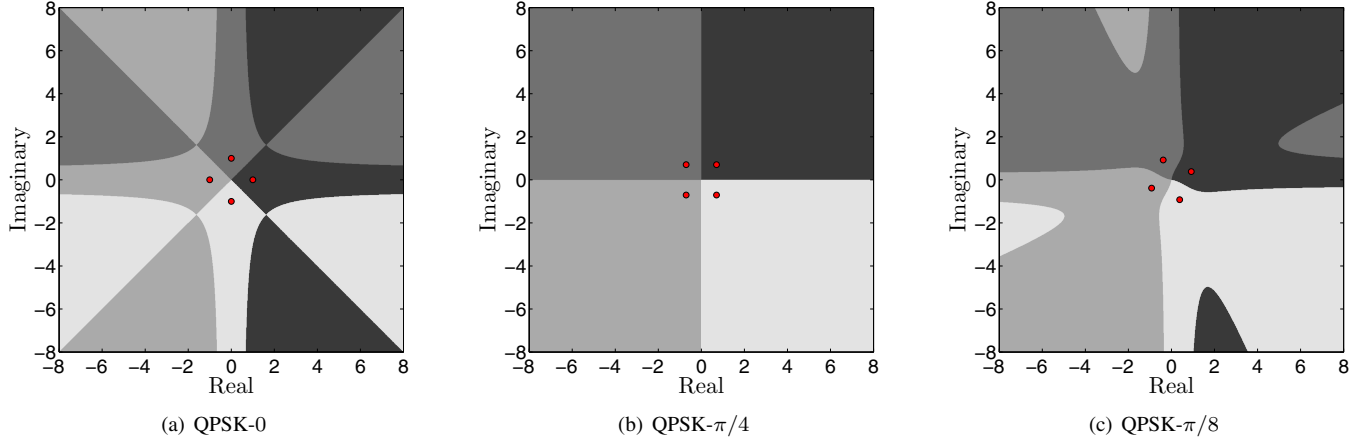


Fig. 4. Optimum decision regions for the Cauchy case ( $\alpha = 1$ ) with independent real and imaginary components of the baseband samples  $Z_b(n)$  for different rotated versions of QPSK.

case, but it will be seen later that they are not efficient in terms of error probability.

## V. SIMULATIONS

In this section we present uncoded bit error rate (BER) and symbol error rate (SER) curves for rotated versions of the QPSK scheme, with the assumption that the complex baseband S $\alpha$ S noise has independent components. However, a suitable equivalent SNR measure is required before we can actually plot these results. We first review the measures available in the literature.

### A. SNR Measures

For digital communication systems in Gaussian noise scenarios, the BER/SER curves are conventionally plotted against the SNR per information bit ( $E_b/N_0$ ), where  $E_b$  is the energy of an information bit and  $N_0/2$  is the two-sided PSD of passband AWGN [1]. Recall, the concept of PSD does not extend to other stable random variables as their respective second moments are infinite. Consequently, one needs a suitable equivalent measure for the non-Gaussian stable case. To our knowledge, there are two different measures that have been proposed in the literature. In essence, there is no difference between the both of them except for an  $\alpha$ -dependent scaling parameter.

The first is based on the *geometric signal-to-noise ratio* (GSNR) approach. This was first proposed in [14] and has been used in [15]–[19]. To explain what the GSNR is, we have to define the *geometric power* of an S $\alpha$ S random variable. The geometric power of an S $\alpha$ S random variable  $X$  is defined as:

$$S_0 = e^{E[\ln |X|]} = \delta C_g^{\frac{1}{\alpha}-1} \quad (39)$$

where  $\delta$  is the scale parameter of  $X$  and  $C_g$  is the exponential of Euler's constant and is approximately 1.7811. It has been proved that  $E[\ln |X|]$  exists [4], where  $X$  is a stable random

variable. The GSNR is then defined as

$$\begin{aligned} \text{GSNR} &= \frac{1}{2C_g} \left( \frac{A}{S_0} \right)^2 \\ &= \frac{1}{2C_g} \left( \frac{A}{\delta C_g^{\frac{1}{\alpha}-1}} \right)^2 \\ &= \frac{A^2}{2\delta^2 C_g^{\frac{2}{\alpha}-1}} \end{aligned} \quad (40)$$

where  $A$  is the *root mean square* (rms) value of the transmitted signal. The GSNR is designed such that for  $\alpha = 2$  (the Gaussian case),  $\text{GSNR} = \text{SNR} = \frac{A^2}{2\delta^2}$ , where  $2\delta^2$  is the variance of the baseband Gaussian noise. The relationship between  $E_b/N_0$  and SNR for our system is given by

$$\frac{E_b}{N_0} = \text{SNR} \times \frac{B}{Bm} \quad (41)$$

where  $m$  is the number of information bits per message symbol. Thus we merely substitute (40) in place of SNR in (41) to get

$$\frac{E_b}{N_0} = \frac{A^2}{\delta_b^2 C_g^{\frac{2}{\alpha}-1}} \times \frac{1}{2m} \quad (42)$$

For the second approach we represent  $E_b/N_0$  for the Gaussian case in terms of the scale parameter  $\delta_b$  instead of  $N_0$ . We may then directly extend this form to other stable random variables as  $\delta_b$  exists for each of them. This measure has been used in [5], [6]. The conversion is done as follows:

$$\frac{E_b}{N_0} = \frac{E_b B}{2\delta_b^2} \quad (43)$$

As  $E_b = \frac{A^2}{mB}$  we further get

$$\frac{E_b}{N_0} = \frac{A^2}{\delta_b^2} \times \frac{1}{2m} \quad (44)$$

On comparing (42) and (44), we see that they only differ by the scale factor  $\frac{1}{C_g^{\frac{2}{\alpha}-1}}$ . For a given  $\alpha$  the scale factor is constant. No expression holds any advantage over the other; in fact, the two different derivations arrive at a 'similar' result,

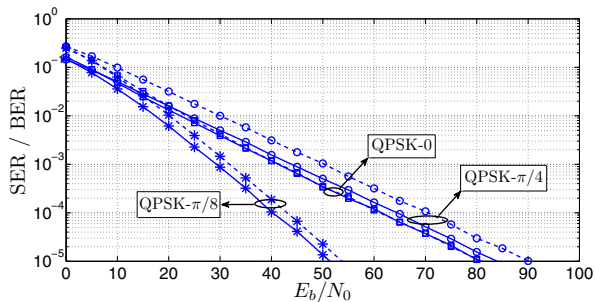


Fig. 5. BER/SER curves for various QPSK schemes are presented under the assumption of independent baseband components for the Cauchy case. Optimal decision boundaries were used for decoding. The dashed lines represent the SER.

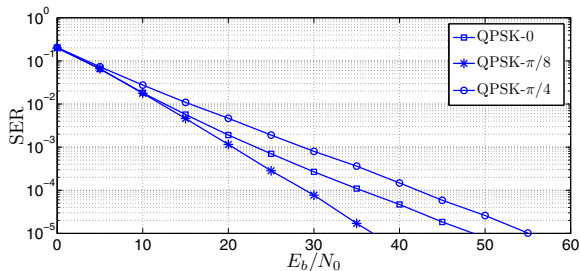


Fig. 6. SER curves for various QPSK schemes are presented under the assumption of independent baseband components for  $\alpha = 1.5$ . Optimal decision boundaries were used for decoding.

showing the consistency of both measures. Some authors prefer using  $\gamma_b^{1/\alpha}$  instead of  $\delta_b$  as the way it was initially proposed in [4], where  $\gamma_b$  is the *dispersion parameter* of the baseband noise. We choose the latter measure for  $E_b/N_0$  for its simpler mathematical form.

### B. BER/SER Curves

Fig. 5 presents the BER/SER curves for the Cauchy case with independent baseband components for rotated versions of QPSK using optimal decision boundaries and Gray coding. The system parameters used to generate these figures are  $f_s = 16$ ,  $f_c = 4$ ,  $B = 1$  and  $M = 800$ . The results were generated for a minimum of 4000 errors for high BER/SER ( $> 10^{-3}$ ) and 1000 errors for low BER/SER. It is observed that when the distribution tails are directed away from the signal points, the BER/SER falls drastically. The QPSK- $\pi/8$  scheme has therefore better BER/SER performance than its QPSK-0 and QPSK- $\pi/4$  counterparts. This reasoning can be intuitively extended to the dependent cases. An interesting observation is that of the SER and BER for QPSK-0. We see that the SER and BER are almost equal as the tails are pointed exactly towards the opposing neighbors for each signal point. Using the same system parameters, we also present SER plots in Fig. 6 for independent components with  $\alpha = 1.5$ .

Fig. 7 depicts the variation of the uncoded SER for the Cauchy case with independent components against the rotation angle assuming QPSK for three different values of  $E_b/N_0$ . Each curve was evaluated using Monte Carlo simulations for a minimum of 3000 errors for selected rotation angles. One can observe that there is an optimum angle (albeit not unique)

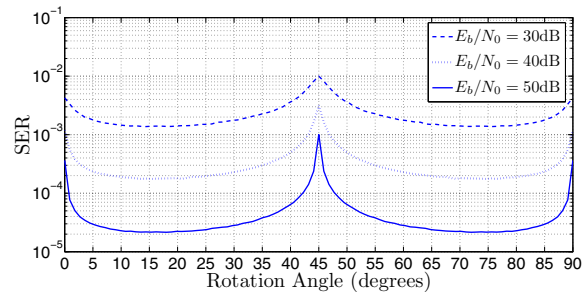


Fig. 7. The SER for the Cauchy case with independent components plotted against the rotation angle for three different values of  $E_b/N_0$ .

for uncoded QPSK transmission that ensures minimum error probability.

## VI. DISCUSSION AND CONCLUSION

In this paper we have analyzed complex baseband noise derived from passband AWS $\alpha$ SN. All baseband noise samples are proven to be IID and any given noise sample is shown to be S $\alpha$ S. The characteristics of the resulting noise are dissimilar to those obtained in the Gaussian case. It has been shown that the real and imaginary components of each sample are generally dependent and non-isotropic. The baseband noise distribution is completely determined by the system parameters. Varying these parameters allows constructing multi-tailed bivariate pdf structures with the tails always being uniformly distributed around the origin. Using the geometry of these distributions, we may intelligently place signal points on constellation maps to achieve more efficient results. Assuming no loss of information in passband-to-baseband conversion, it is argued that the case of independent real and imaginary baseband noise components, i.e.  $f_s/f_c = 4$ , delivers best error performance when the I and Q channels are separately decoded. Further still, if the noise is non-Gaussian then the resulting distribution has to be non-isotropic. Focusing on such a system, error rates were evaluated for various rotated versions of QPSK. It was shown that the SER/BER were heavily influenced by the rotation angle due to the noise being non-isotropic. Further still, with the exception of QPSK- $\pi/4$ , the optimal decision regions for all rotated QPSK constellations with independent baseband S $\alpha$ S components depend on the  $E_b/N_0$ . The work presented in this paper provides an understanding of baseband S $\alpha$ S noise and creates a platform necessary to develop effective baseband communication techniques in impulsive noise scenarios.

It is well known in the literature that non-linear techniques are more robust and effective in negating the adverse influence of impulsive noise [14], [20]–[23]. The *myriad filter*, first introduced in [14], [20], is a robust estimator derived from the *generalized maximum likelihood estimator* (or M-estimator) framework. The myriad filter outputs an unbiased robust estimate of the location parameter  $\mu$  of a set of input samples that are immersed in impulsive noise. This estimate is termed as the *myriad* of the input samples. Associated with the computation of the myriad is a free-tunable parameter ‘ $k$ ’, termed as the *linearity parameter*. The myriad filter demonstrates optimality properties if the impulsive noise is modeled by the S $\alpha$ S family

of distributions [14], [21], [22]. If the noise samples are IID and S $\alpha$ S with  $\alpha = 1$  (Cauchy), the myriad outputs the ML estimate of  $\mu$  of the sample set if  $k$  is set to the scale parameter  $\delta$  of the noise. In [22], it has been shown that the myriad outputs optimal estimates of  $\mu$  for shifted S $\alpha$ S distributions for  $\alpha = 2$ ,  $\alpha = 1$  and  $\alpha \rightarrow 0$  with  $k \rightarrow \infty$ ,  $k = \delta$  and  $k \rightarrow 0$ , respectively. These optimal points of operation have been termed as the  $\alpha - k$  triplet.

A prerequisite for obtaining a reliable myriad estimate of  $\mu$  of a shifted S $\alpha$ S distribution is the independence of noise samples. Fig. 1 depicts the passband-to-baseband conversion process. One possible way of incorporating the myriad filter in the model is to insert it between the linear filter and downsampler block. To estimate any baseband symbol  $\vec{Z}_b(n)$ ,  $f_s$  samples of  $\vec{Z}(n)$  are available to the myriad filter as input. To ensure that the noise samples  $\vec{Z}(n)$  are almost independent, the low-pass filter is replaced by a linear filter that nullifies the signal component of  $\vec{Z}^+(n)$  centered at  $-2f_c/f_s$  while maintaining as much out-of-band noise as possible. The myriad filter in conjunction with the downsampler is in essence a *matched myriad filter* (MMyF) [14]. Further still, with  $f_s/f_c = 4$ , the real and imaginary components of all upsampled baseband symbols  $\vec{Z}(n)$  are independent. Passing this to the MMyF ensures that the components of  $\vec{Z}_b(n)$  are still be independent and hence non-isotropic. The relationship of the carrier and passband sampling frequencies with the noise anisotropy in the linear case can be extended to the design of non-linear communication systems in impulsive noise. The decision boundaries and error performance of the non-linear receiver will also depend on the rotation angle of the constellation, as seen in the case of the linear receiver.

The work in this paper is limited to uncoded systems. To enhance performance one could introduce an error-correction code as part of the system. Codes developed specifically for AWGN scenarios will provide added performance but still would not be optimal. Future work will be directed along the lines of developing good codes for impulsive noise environments. Combined with a non-linear technique as the myriad filter, the resulting system would provide excellent error performance relative to the uncoded performance in a conventional passband-to-baseband scenario. The results and insight presented in this paper are equally important as they provide invaluable insight in tackling the problems that lie ahead.

## REFERENCES

- [1] J. Proakis, *Digital Communications*, 4th edition. McGraw-Hill, 2000.
- [2] J. P. Nolan, *Stable Distributions - Models for Heavy Tailed Data*. Birkhauser, 2012, Chapter 1, in progress. Available: [academic2.american.edu/~jpnolan](http://academic2.american.edu/~jpnolan)
- [3] G. Samorodnitsky and M. S. Taqqu, *Stable Non-Gaussian Random Processes: Stochastic Models with Infinite Variance*. Chapman & Hall, 1994.
- [4] C. L. Nikias and M. Shao, *Signal Processing with Alpha-Stable Distributions and Applications*. Chapman-Hall, 1996.
- [5] M. Chitre, J. Potter, and S.-H. Ong, "Optimal and near-optimal signal detection in snapping shrimp dominated ambient noise," *IEEE J. Oceanic Eng.*, vol. 31, no. 2, pp. 497–503, Apr. 2006.
- [6] M. Chitre, J. Potter, and S. Ong, "Viterbi decoding of convolutional codes in symmetric alpha-stable noise," *IEEE Trans. Commun.*, vol. 55, no. 12, pp. 2230–2233, Dec. 2007.

- [7] M. Chitre, J. Potter, and O. Heng, "Underwater acoustic channel characterisation for medium-range shallow water communications," in *Proc. 2004 MTTT/IEEE TECHNO-OCEAN*, vol. 1, pp. 40–45.
- [8] J. H. McCulloch, *Numerical Approximation of the Symmetric Stable Distribution and Density*. Birkhauser Boston Inc., 1998, pp. 489–499.
- [9] J. P. Nolan, "Numerical calculation of stable densities and distribution functions," *Commun. Statistics - Stochastic Models*, vol. 13, no. 4, pp. 759–774, 1997.
- [10] E. Kuruoglu, P. Rayner, and W. Fitzgerald, "A near-optimal receiver for detection in alpha-stable distributed noise," in *Proc. 1998 IEEE SP Workshop Statistical Signal Array Process.*, pp. 419–422.
- [11] E. Kuruoglu, W. Fitzgerald, and P. Rayner, "Near optimal detection of signals in impulsive noise modeled with a symmetric alpha-stable distribution," *IEEE Commun. Lett.*, vol. 2, no. 10, pp. 282–284, Oct. 1998.
- [12] A. Swami, "Non-Gaussian mixture models for detection and estimation in heavy-tailed noise," in *Proc. 2000 IEEE Int. Conf. Acoustics, Speech, Signal Process.*, vol. 6, pp. 3802–3805.
- [13] A. Papoulis and U. S. Pillai, *Probability, Random Variables and Stochastic Processes*. McGraw-Hill, 2001.
- [14] J. G. Gonzalez, "Robust techniques for wireless communications in non-Gaussian environments," Ph.D. dissertation, University of Delaware, Newark, DE, USA, 1997.
- [15] T. Chuah, B. Sharif, and O. Hinton, "Nonlinear decorrelator for multiuser detection in non-Gaussian impulsive environments," *Electron. Lett.*, vol. 36, no. 10, pp. 920–922, May 2000.
- [16] S. Yoon, I. Song, and S. Y. Kim, "Code acquisition for DS/SS communications in non-Gaussian impulsive channels," *IEEE Trans. Commun.*, vol. 52, no. 2, pp. 187–190, Feb. 2004.
- [17] T. C. Chuah, "On Reed-Solomon coding for data communications over power-line channels," *IEEE Trans. Power Delivery*, vol. 24, no. 2, pp. 614–620, Apr. 2009.
- [18] M. Shafieipour, H. S. Lim, and T. C. Chuah, "Decoding of turbo codes in symmetric alpha-stable noise," *ISRN Signal Process.*, vol. 2011, article ID 683972, 2011.
- [19] J. Gonzalez, J. Paredes, and G. Arce, "Zero-order statistics: a mathematical framework for the processing and characterization of very impulsive signals," *IEEE Trans. Signal Process.*, vol. 54, no. 10, pp. 3839–3851, Oct. 2006.
- [20] J. Gonzalez and G. Arce, "Weighted myriad filters: a robust filtering framework derived from alpha-stable distributions," in *Proc. 1996 IEEE International Conf. Acoustics, Speech, Signal Process.*, vol. 5, pp. 2833–2836.
- [21] —, "Optimality of the myriad filter in practical impulsive-noise environments," *IEEE Trans. Signal Process.*, vol. 49, no. 2, pp. 438–441, Feb. 2001.
- [22] J. G. Gonzalez and G. R. Arce, "Statistically-efficient filtering in impulsive environments: weighted myriad filters," *EURASIP J. Appl. Signal Process.*, vol. 2002, pp. 4–20, Jan. 2002.
- [23] G. Arce, *Nonlinear Signal Processing: A Statistical Approach*. Wiley-Interscience, 2005.



**Ahmed Mahmood** (S'11) is currently a doctoral candidate at the Department of Electrical & Computer Engineering, National University of Singapore. He received his B.Eng and M.Eng degrees in electrical engineering from the National University of Sciences and Technology, Pakistan. His current research interests involve underwater communication, signal processing, channel modelling, and error correction coding for impulsive noise.



**Mandar Chitre** (M'03-SM'12) received the B.Eng. (Hons) and M.Eng. degrees in electrical engineering from the National University of Singapore (NUS), Singapore, a M.Sc. degree in bioinformatics from Nanyang Technological University (NTU), Singapore, and a Ph.D. degree from NUS. From 1997 to 1998, he worked with the Acoustic Research Laboratory (ARL), NUS, in Singapore, as a Research Engineer. From 1998 to 2002, he headed the technology division of a regional telecommunications solutions company. In 2003, he rejoined ARL,

initially as Deputy Head (Research) and now as Head of the laboratory. He also holds a joint appointment with the Department of Electrical & Computer Engineering at NUS as an Assistant Professor. His current research interests are underwater communications, autonomous underwater vehicles, and underwater signal processing.

Dr. Chitre has served on the technical program committees of the IEEE OCEANS, WUWNet, DTA and WSS conferences and has served as reviewer for numerous international journals. He was chairman of the student poster committee for IEEE OCEANS'06 in Singapore. In the past years, he has served as the vice chairman, secretary, and treasurer for the IEEE OES (Singapore Chapter) and is currently the IEEE technology committee co-chair of underwater communication, navigation, and positioning. He also serves as a technical co-chair for the IEEE ICCS'12 conference and as chairman for the Singapore autonomous underwater vehicle challenge organized by IEEE OES.



**Armand** (M'00-SM'07) received the B.Eng. and Ph.D. degrees in electrical engineering from the University of Bristol, U.K., in 1995 and 1999, respectively. In Dec. 2000, he joined the faculty at the Department of Electrical & Computer Engineering, National University of Singapore, where he is now an Associate Professor. His research interests include symbolic computation and coding theory with particular focus on coding for channels with synchronization errors.